# State transition of stable nanobubbles to unstable microbubbles on homogeneous surfaces

Binghai Wen [1], Yongcai Pan [1], Lijuan Zhang [2], Shuo Wang [3], Limin Zhou [2,*], Chunlei Wang [4,5,†] and Jun Hu [4,5]

[1] *School of Physical Science and Technology, Guangxi Normal University, Guilin 541004, China*
[2] *Shanghai Synchrotron Radiation Facility, Shanghai Advanced Research Institute, Chinese Academy of Sciences, Shanghai 201204, China*
[3] *Julong college, Shenzhen Technology University, Shenzhen 518118, China*
[4] *Zhangjiang Lab, Interdisplinary Research Center, Shanghai Advanced Research Institute, Chinese Academy of Sciences, Shanghai 201210, China*
[5] *Key Laboratory of Interfacial Physics and Technology, Shanghai Institute of Applied Physics, Chinese Academy of Sciences, Shanghai 201800, China*

(Received 24 December 2021; accepted 20 September 2022; published 4 October 2022)

Experiments have revealed the remarkably long lifetime of surface nanobubbles, but experiments have also demonstrated the diffusive instability of bubbles above micrometers; thus a physical understanding on the transition of bubbles stability is in urgent need. Herein, we develop a model to capture the state transition from stable nanobubbles to unstable microbubbles on homogeneous surfaces. The transition explains the typical long lifetime, limited height, and small contact angle of surface nanobubbles observed in experiments. The phase diagram shows that the bubble size and dissolved gas saturation determine the dynamic behaviors of surface bubbles, namely growth, stability, shrinkage, or dissolution.

DOI: 10.1103/PhysRevFluids.7.103601

## I. INTRODUCTION

Surface nanobubbles, which are spherical-cap gaseous domains with nanoscale thickness attached on immersed substrates, exhibit a surprisingly long lifetime, surviving up to days and weeks [1–6]. They have a special flat morphology; typically, the heights are less than 100 nm, and the gas-side contact angles are around 20° and appear to be weakly dependent on substrate wettability [7–14]. The remarkable stability has perplexed researchers for nearly two decades, because it contradicts the widely accepted Epstein-Plesset theory, which was established for bulk bubbles and then adopted for surface bubbles described by the curvature radius [1,5,15]. This theory suggests that all gas bubbles are diffusively unstable in practical situations, experiencing either shrinkage to dissolution or unbounded growth [5,16,17]. Notably, the theoretical prediction is in excellent agreement with experiments on bubble radii down to micrometers [5,18]. For nanosized bubbles, it gives the lifetime corresponding to the diffusion timescale $\tau \sim R_0^2 \rho_g/(Dc_s)$ and suggests that a typical nitrogen nanobubble with the initial radius $R_0 = 100$ nm must dissolve within 100 $\mu s$, where $\rho_g$ is the gas density, $c_s$ is the gas solubility and $D$ is the diffusion constant for the gas in the liquid [1,15]. Thus, although the stability of surface nanobubbles has several well understandings [19–23],

*Corresponding authors: zhoulimin@zjlab.org.cn
†wangchunlei@zjlab.org.cn

 

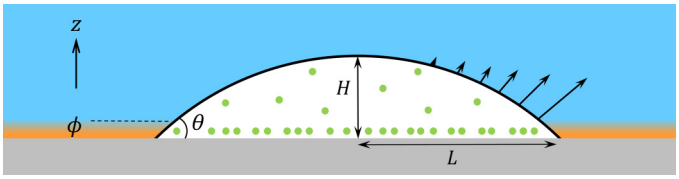


FIG. 1. Schematic diagram of a surface nanobubble.

there is an imminent need to theoretically describe the state transition between the remarkable stability of nanobubbles and the general instability of microbubbles.

The stability of surface bubbles requires gas diffusive equilibrium at the liquid-bubble interface to maintain the volume at constant; meanwhile it also requires mechanical equilibrium at the three phase contact line to keep the bubble immobile. Contact line pinning was considered to be a prerequisite to stabilize surface nanobubbles [19,24,25]. Besides settling the mechanical equilibrium readily, contact line pinning compels a nanobubble to reduce the curvature and Laplace pressure when its volume decreases, and then promotes its stability [26]. But pinning cannot work alone to prevent the bubble's shrinkage and dissolution, because the Laplace pressure tends to press any gas out of bubbles [1,20,27]. Gas oversaturation of the ambient liquid effectively counteracts the gas leakage from the nanobubble, even though it has already been reduced to a small amount by the pinning effect [20,27,28]. Nevertheless, experiments indicated that nanobubbles could survive in an open or degassed liquid [25,29,30]. An attractive potential was introduced to enrich the dissolved gas adjacent to hydrophobic substrate and stabilize nanobubbles in undersaturated environments [21,31–35]. Then, by considering gas transport as the bulk liquid equilibrated with the external environment, the stability and dynamics of surface nanobubbles were consistent with experimental response timescale [24,36]. Although contact line pinning together with oversaturation or hydrophobic potential could effectively stabilize surface nanobubbles, experiments have demonstrated that nanobubbles could be readily moved on PFOTS, PDMS or polymer brush surfaces by using an AFM tip [13,37,38]. These phenomena agree with the simulations, which also supported that contact line pinning was not strictly required for the mechanical equilibrium of surface nanobubbles [23,39]. Recently, the adsorption of gas molecules at the substrate beneath surface nanobubbles was taken into account to lower the energy of the solid-gas interface and explain the flat nanobubble morphology [22]. The diffusive equilibrium is ignored by assuming the liquid-bubble interface would be impermeable.

In this paper, we propose a model that captures bubble dynamics on homogeneous substrate without contact line pinning, which can simultaneously achieve both the diffusive and mechanical equilibriums, and uniformly illustrate the nanobubble stability and the instability of larger bubbles above microscale.

## II. MODEL

Figure 1 presents a nanobubble on a homogeneous surface with a spherical cap shape parameterized by the footprint radius $L$, the bubble height $H$, and the gas-side contact angle $\theta$. The Laplace equation gives the pressure inside the nanobubble $P = P_0 + 2\gamma_{lg}/R$, where $P_0$ is atmospheric pressure, $R$ is the curvature radius, and $\gamma_{lg}$ is the liquid-gas surface tension. The gas concentration at the liquid-bubble interface can be given by Henry's law $c(t) = c_s P(t)/P_0$ [20].

The gas diffusion from a surface nanobubble is analogous to the evaporation of a pinned drop [40], which was exactly solved by Popov [41]. Incorporating Henry's law into Popov's solution, Lohse and Zhang derived the mass change of a pinned nanobubble in a supersaturated liquid [20],

$$\frac{dM}{dt} = -\pi L D c_s f(\theta)\left(\frac{2\gamma_{lg}}{LP_0}\sin\theta - \zeta\right), \tag{1}$$

where $\zeta = c/c_s - 1$ is the gas oversaturation of the environmental liquid, and the geometric term depends on the gas-side contact angle,

$$f(\theta) = \frac{\sin\theta}{1+\cos\theta} + 4\int_0^\infty \frac{1+\cosh 2\theta\xi}{\sinh 2\pi\xi}\tanh\left[(\pi-\theta)\xi\right]d\xi. \tag{2}$$

Once the diffusive equilibrium appears, namely $dM/dt = 0$, the contact angle is dependent on the oversaturation by $\sin\theta = LP_0\zeta/2\gamma_{\rm lg}$. Brenner *et al.* [31] used a short-ranged attraction potential $\phi_0$ to reach the dynamic equilibrium of surface nanobubble. Tan *et al.* [21] introduced the potential into the pinning model and further explained the experimental observations that surface nanobubbles could survive in undersaturated environments [29,30]. The attraction potential induced a supersaturated gas reservoir even if the bulk liquid is undersaturated and then changed the distribution of dissolved gas oversaturation adjacent to the substrate [21,31,35,42],

$$\zeta(z) = \frac{c_\infty}{c_s}\exp\left(-\frac{\phi_0 e^{-z/\lambda}}{k_B T}\right) - 1, \tag{3}$$

where $\lambda \sim 1$ nm is the characteristic distance of the interaction. The Epstein-Plesset theory and experiments suggest that bubbles respond dynamically to local changes in the dissolved gas concentration in the surrounding liquid [18,21,43]. This supersaturated layer raises the localized concentration on the liquid side and compensates for the gas leakage in the upper part of nanobubbles. Since the gas reservoir induced by the hydrophobic attraction concentrates very close to the substrate [21], its influence on the liquid-gas interface energy can be ignored.

However, pinning is helpful to stabilize a surface nanobubble instead of a prerequisite [23,37–39]. In fact, the Popov's equation does not strictly require contact line pinning [41], which is just necessary to form a stain ring during drop evaporation [40]. Hence the Popov's equation can be adopted to calculate the dynamics of a nanobubble without pinning, but the mechanical equilibrium must be settled first.

Essentially, the mechanical equilibrium at an unpinned contact line is illuminated by the Young equation, which relates the interface energies to the contact angle [44,45]. Petsev *et al.* considered that the adsorption of gas molecules to the substrate lowered the solid-gas interface energy and explained the flat morphology of nanobubbles from a thermodynamic perspective [22]. The adsorption effect is described by the Langmuir adsorption isotherm, which is thermodynamically equivalent to the Szyszkowski equation [22,46],

$$\gamma_{\rm sg}^*(P) = \gamma_{\rm sg}^0 - \frac{k_B T}{b}\ln(1+KP), \tag{4}$$

where $K$ is the equilibrium adsorption constant, $b$ is the cross-sectional area of a single adsorbing molecule, $\gamma_{\rm sg}^0$ is the surface tension of the solid-gas interface in a vacuum or absence of adsorption. Combining Eq. (4) and the Young equation $\gamma_{\rm sg}^* - \gamma_{\rm sl} + \gamma_{\rm lg}\cos\theta = 0$ gives a general expression for the influence of gas adsorption [22],

$$\gamma_{\rm sg}^0 - \gamma_{\rm sl} + \gamma_{\rm lg}\cos\theta - \frac{k_B T}{b}\ln(1+KP) = 0, \tag{5}$$

where $\gamma_{\rm sl}$ is the solid-liquid surface tension. This adsorption model does not settle the diffusive equilibrium but assumes no transfer of gas molecules across the liquid-bubble interface [22].

Molecular dynamics simulations showed that the timescale that thermal motion of molecules equilibrates a contact angle is within nanoseconds [23,47,48], which is more than three orders of magnitude faster than the diffusion timescale. From the perspective of diffusion, surface nanobubbles always retain the mechanical equilibrium during dynamic growth or shrinkage. Substituting the solid-gas surface tension at atmospheric pressure $\gamma_{\rm sg} = \gamma_{\rm sg}^*(P_0)$ into Eq. (5) gives the contact angle

with the mechanical equilibrium,

$$\cos\theta = \cos\theta_0 + \frac{k_B T}{b\gamma_{\rm lg}} \ln\left(\frac{1+KP}{1+KP_0}\right), \tag{6}$$

where $\theta_0$ indicates the wettability of the substrate at atmospheric pressure. Replacing the contact line pinning by the adsorption effect, namely constraining the real time contact angle by Eq. (6), we can derive the dynamic equation to evolve a bubble on a homogeneous surface

$$\frac{dM}{dt} = -\frac{\pi L D c_s}{H} f(\theta)\left[\frac{2\gamma_{\rm lg}}{P_0}\left(1-\cos\theta_0 - \frac{k_B T}{b\gamma_{\rm lg}} \ln\frac{1+KP}{1+KP_0}\right) - \int_0^H \zeta(z)dz\right]. \tag{7}$$

When the evolution achieves $dM/dt = 0$, this derives the equilibrium equation,

$$\cos\theta_e \equiv 1 - \frac{P_0}{2\gamma_{\rm lg}}\int_0^H \zeta(z)dz = \cos\theta_0 + \frac{k_B T}{b\gamma_{\rm lg}} \ln\left(\frac{1+KP}{1+KP_0}\right), \tag{8}$$

which ensures the diffusive and mechanical equilibriums simultaneously. Furthermore, it demonstrates that nanobubbles can be stabilized on a homogeneous surface, as long as the contact angle from diffusive equilibrium is equal to that required by mechanical equilibrium, without the help of pinning, softness, roughness or heterogeneity.

## III. RESULTS

We consider a typical case of a bubble system at ambient conditions. The parameters are referred to the literature by Lohse and Zhang [20], Tan *et al.* [21] and Petsev *et al.* [22], viz., $D = 2 \times 10^{-9}\,\mathrm{m^2/s}$, $c_s = 0.017\,\mathrm{kg/m^3}$, $\rho_g = 1.165\,\mathrm{kg/m^3}$, $\lambda = 1$ nm, and $b = 7.548 \times 10^{-2}\,\mathrm{nm^2}$ [22]. Both $\theta_0$ and $\phi_0$ relate to the wettability of the substrate, and the analysis shows that their relationship is approximately linear [35]. Thus, we use a linear connection here; a neutral substrate, which is equal to that in Lohse and Zhang model [20,21], has a zero potential, and $\theta_0 = 60^\circ$ corresponds to $\phi = -2$, where $\phi = \phi_0/(k_B T)$. The adsorption constants of different substrates span a broad spectrum of magnitudes, and $K$ is typically between $1.0 \times 10^{-6} - 1.9 \times 10^{-3}\,\mathrm{Pa^{-1}}$ for $N_2$, $O_2$, and $CO_2$ adsorbing to HOPG, MG-MOF, or $Fe_2$ [22]. We choose a representative value of $K = 1.0 \times 10^{-5}\,\mathrm{Pa^{-1}}$ for qualitative experimental comparisons.

The dynamic equation (7) and equilibrium equation (8) depict the phase diagram of bubble dynamics on a homogeneous surface, as shown in Fig. 2. We solve Eq. (8) for the footprint radius as a function of the oversaturation on the substrate with $\theta_0 = 60^\circ$. The functional curve begins at $L = 10$ nm and $\zeta = -0.58$. Since the corresponding height has already been less than 1 nm, the gaseous domain could be viewed as a gas nucleation. The curve has an apparent turning point at $\zeta = 1.44$ and $L = 267$ nm, which separates the curve into the lower solid and upper dashdot parts. Above the turning point, the dashdot curve gradually approaches the line $\zeta = 0$ as the bubble grows to more than microns, because a large bubble has a low Laplace pressure and then the adsorption effect becomes weaker and weaker. The function curve together with the three lines $\zeta = -0.58$, 0, and 1.44 partition the phase diagram into five sections in Fig. 2(a). Then, we solve Eq. (7) to investigate the bubble dynamics in each section, and five typical nanobubbles are selected correspondingly. The initial footprint radii are $L = 500$ nm for the section I–III and 20 nm for the section IV − V. During the dynamic evolutions, the oversaturation of the bulk liquid keeps $\zeta = -0.8,\ -0.2,\ 0.2,$ 1.0, and 2.0, respectively. Fig. 2(b) presents that the nanobubble in the section I (blue) shrinks until it dissolves completely, and this process is accelerative since the Laplace pressure diverges as the curvature radius decreases. The nanobubbles in the section II (green) and III (magenta) also shrink, but they finally reach the stable state located at the solid curve; notwithstanding, the section III has an upper limit given by the dashdot curve. The nanobubble in the section IV (yellow) grows to the stable state at the solid curve, while that in the section V (gray) presents an unbounded growth up to microscale.

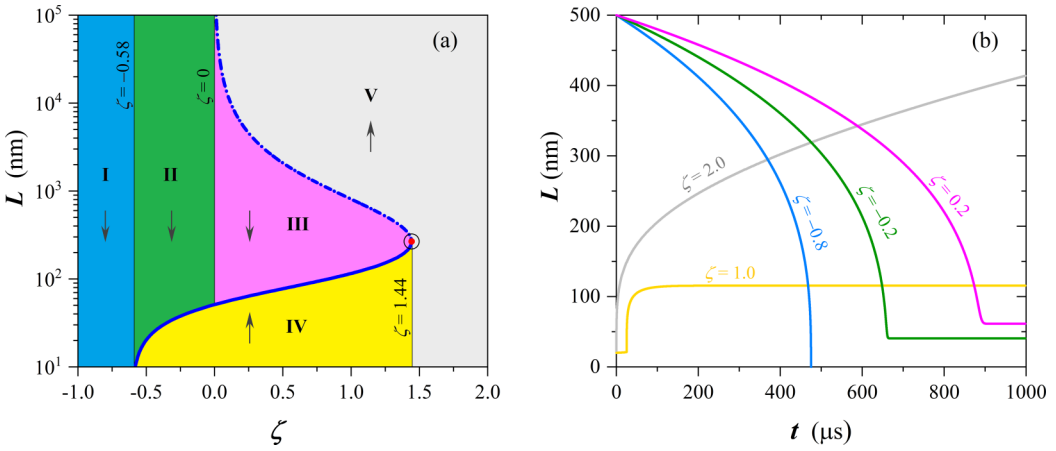


FIG. 2. (a) The phase diagram of bubble dynamics on a homogeneous substrate with $\theta_0 = 60^\circ$. The turning point at $\zeta = 1.44$ divides the curve into the solid and dashdot parts, which indicate the stable and unstable equilibrium states of surface bubbles, respectively. The curve together with the lines $\zeta = -0.58$, 0, and 1.44 partition the diagram into five sections. The arrows indicate the trends of the bubble evolution in each section. (b) The dynamic evolutions of five typical nanobubbles in each section. The colors of the lines represent the sections they belong to. The evolution of the nanobubble in the section IV (yellow) has been postponed by 25 $\mu$s in order to avoid data overlap.

The phase diagram manifests that the dynamics of nanobubbles are determined by their sizes and gas oversaturation, and exhibits the behaviors of growth, stability, shrinkage, or dissolution. As comparisons, the phase diagrams of nanobubbles on the substrates with $\theta_0 = 50^\circ$ and $\theta_0 = 70^\circ$ are drawn in Fig. 3. Figures 3(a) and 3(c) present that the surface hydrophobicity significantly influences the division of the sections. As the substrate of $\theta_0 = 50^\circ$ is more hydrophobic, it can stabilize nanobubbles in a lower oversaturation. Thus, the curve moves to the left, the section I is compressed and the section II expands. Whereas, the substrate of $\theta_0 = 70^\circ$ is less hydrophobic and requires a larger oversaturation to stabilize nanobubbles. Thus, the section II is compressed, the section I expands and swallows the section II gradually. Figures 3(b) and 3(d) present the dynamic behaviors of surface nanobubbles in different sections, including growth, stability, shrinkage or dissolution. The evolutions of the nanobubbles in the section IV (yellow) have been postponed by 50 $\mu$s in order to avoid data overlap.

Then, we distinguish the stable and unstable equilibrium states of nanobubbles indicated by the lower solid curve and the upper dash-dot curve, respectively. Two sets of evolutions with $\theta_0 = 60^\circ$ are performed to investigate the bubble dynamics around the curve. For the solid part, five nanobubbles are selected with the oversaturation $\zeta = 1$ and the initial footprint radius $L = 20$, 50, 100, 150, and 200 nm, respectively. Figure 4(a) presents that all five cases evolve and reach the equilibrium point $L = 116$ nm on the solid curve, while the relevant height and contact angle are $H = 9$ nm and $\theta = 8.63^\circ$. Importantly, the nanobubbles on both sides must converge to the solid curve; that is to say, even with some perturbations, they will quickly return to the stable state. Therefore, the solid curve represents the stable equilibrium of nanobubbles on a homogeneous substrate. For the dash-dot curve in the phase diagram, we select the nanobubble with $L = 500$ nm and $\zeta = 1.27$ on the curve and the other four nanobubbles surrounding it. Figure 4(b) presents that the nanobubbles on both sides always deviate from the dash-dot curve, whereas the nanobubble curve keeps unchanged. Since the four surrounding nanobubbles have less than 1% difference in the footprint radius or oversaturation relative to the central one, the equilibrium state represented by the central one can be easily broken by a slight perturbation from the bubble size or gas

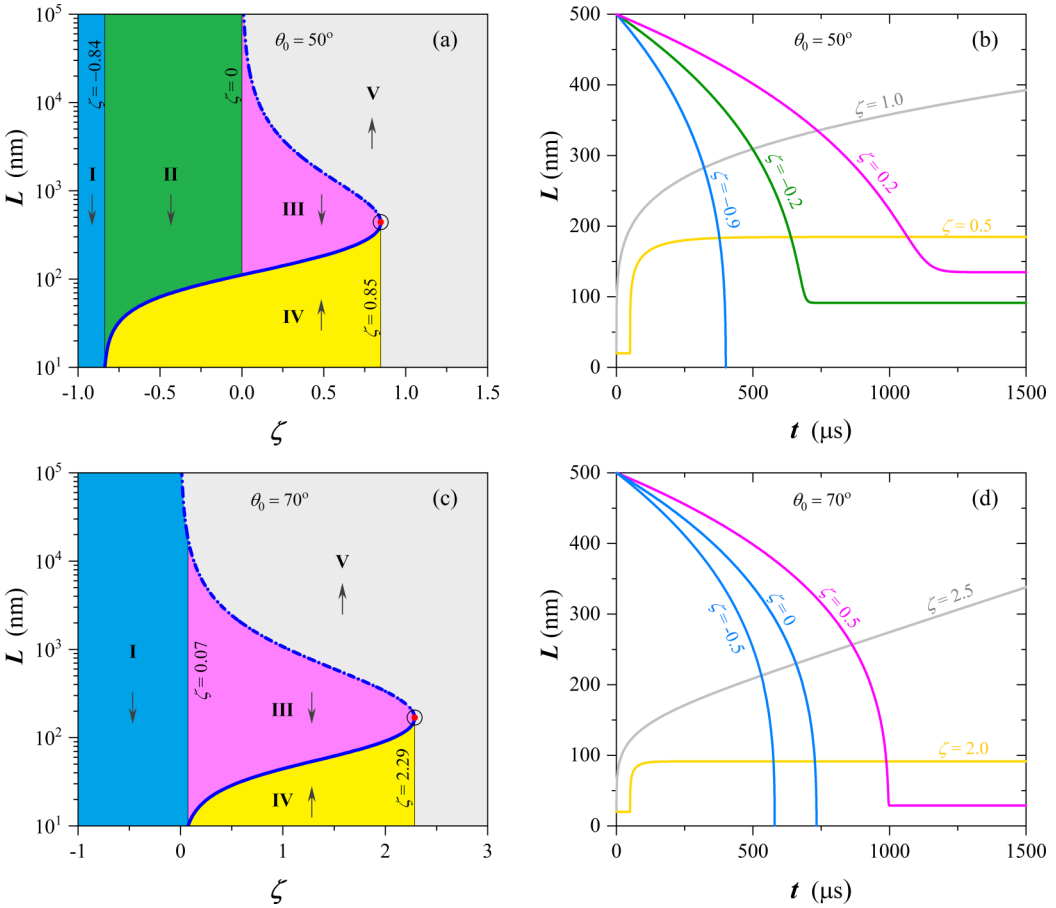


FIG. 3. The phase diagram of bubble dynamics on homogenous substrates with (a) $\theta_0 = 50^\circ$ and (c) $\theta_0 = 70^\circ$. (b) and (d) are the dynamic evolutions of five typical nanobubbles and the colors of the lines represent the sections they belong to.

concentration. Therefore, the dash-dot curve represents an unstable equilibrium of nanobubbles on a homogeneous substrate.

These analyses demonstrate that the present theory uniformly describes the stability of nanobubbles, which has been confirmed by experiments [8,25,30,49], and the instability of bubbles with larger sizes up to microscale, which has been predicted by the Epstein-Plesset theory and validated by microscope observations [5,16–18]. The section III connects the solid and dashdot curves simultaneously, thus, for a given oversaturation, bubbles on a homogeneous surface can be in the stable or unstable equilibrium state; the former corresponds to the free energy minimum, while the latter suggests the free energy maximum of the bubble system [26,50]. It is the turning point that indicates the state transition of surface bubbles from the stable equilibrium to the unstable equilibrium. Except the equilibriums represented by the curve, nanobubbles at the rest of the phase diagram are in a nonequilibrium state, and their stabilizations *in situ* must get help from the contact line pinning.

Next, we investigate the influence of surface wettability on the nanobubble stability. Figure 5(a) presents the heights of equilibrium bubbles as functions of the oversaturation. With the decrease of surface hydrophobicity indicated by $\theta_0$, the curves of stable equilibrium become more and more to the right. This suggests that the larger oversaturation is required to equilibrate nanobubbles on

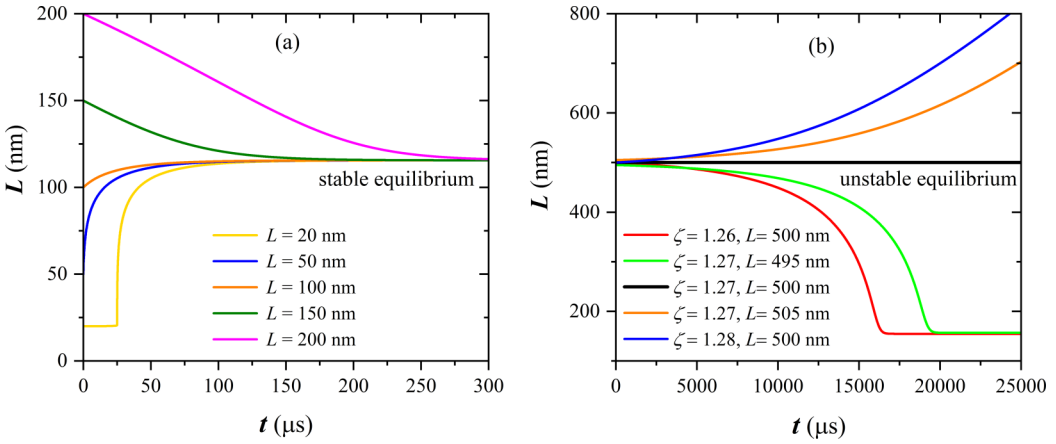


FIG. 4. The comparison of the dynamic evolutions of nanobubbles around the stable and unstable equilibriums. (a) The dynamic evolutions of the five nanobubbles on both sides of the solid curve in Fig. 2. The oversaturation takes $\zeta = 1$ and the initial footprint radii are $L = 20$, 50, 100, 150, and 200 nm, respectively. All of them converge to the point $L = 116$ nm on the solid curve and achieve a stable equilibrium state. (b) The dynamic evolutions of the five nanobubbles adjacent to the dashdot curve in Fig. 2. The central nanobubble with $L = 500$ nm and $\zeta = 1.27$ is on the dashdot curve, while the others around it have less than 1% difference in the footprint radius or oversaturation. Since all surrounding nanobubbles deviate from it, the central nanobubble represents an unstable equilibrium state.

lower hydrophobic substrates. Above the turning points, as bubbles grow gradually up to microscale, the oversaturation required by the unstable equilibrium on every substrate approaches $\zeta = 0$. This is consistent with the Epstein-Plesset equation and experiments, which confirmed that, above micrometers, bubbles could only be equilibrated in the solvent with gas saturation concentration [5,16,18]. Meanwhile, each bubble contact angle touches the intrinsic contact angle $\theta_0$, as shown in Fig. 5(b). These reflect the decrease of the Laplace pressure and the weakening of the adsorption effect in larger bubbles. Furthermore, the turning points give the height and contact angle maximums

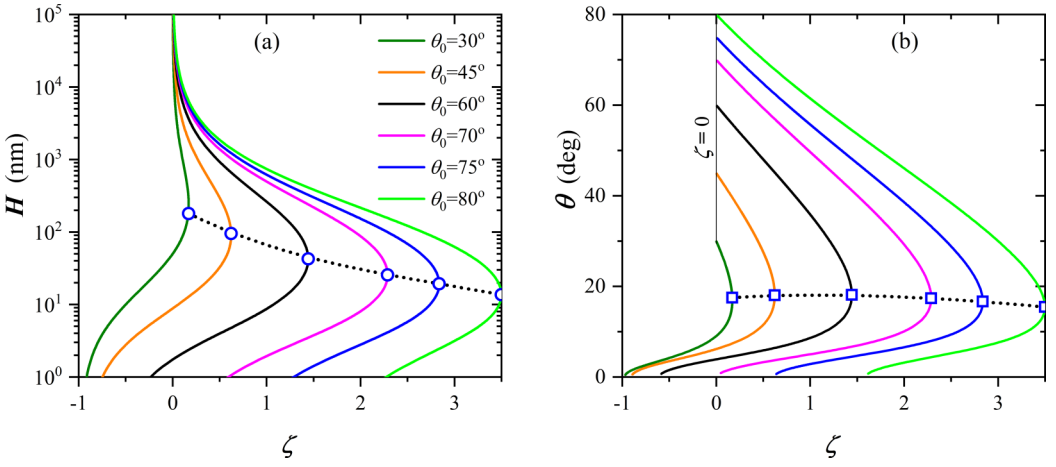


FIG. 5. (a) The heights and (b) the contact angles of equilibrium bubbles as functions of the oversaturation on the substrates with various wettability. The turning points of the bubble heights and contact angles are marked by the circles in (a) and squares in (b), respectively.

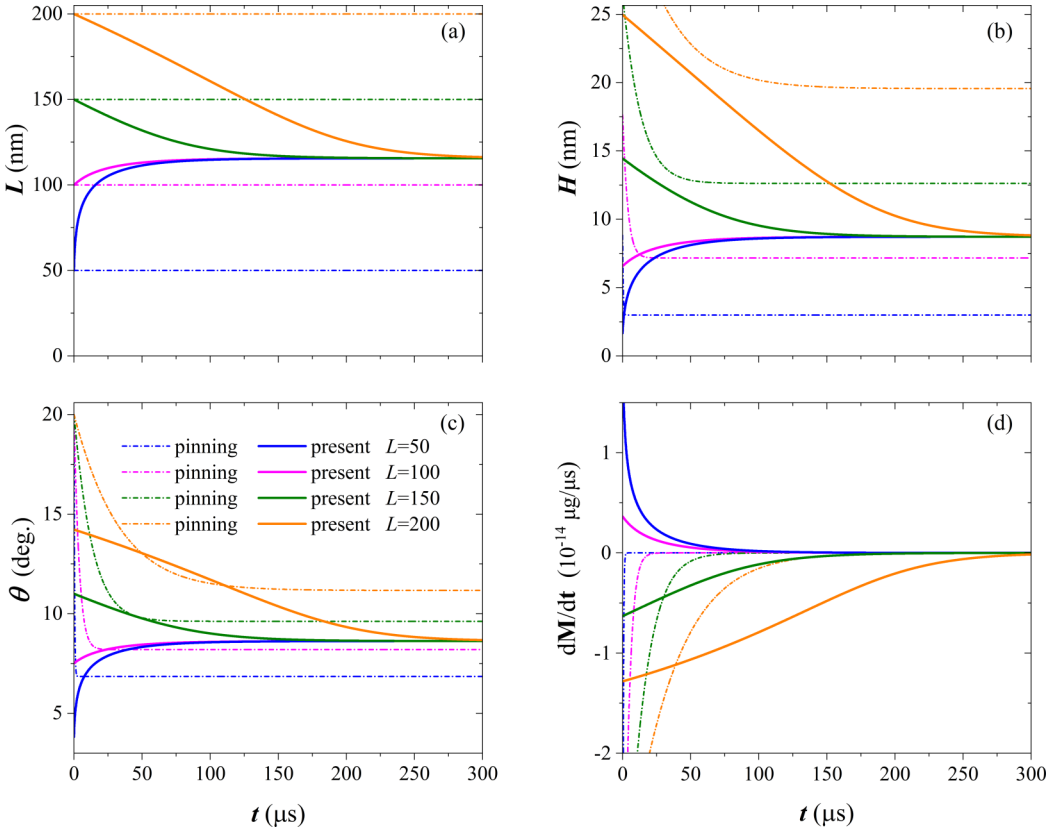


FIG. 6. The dynamic evolutions of surface nanobubbles computed by the present study and the pinning model: (a) footprint radii, (b) bubble heights, (c) contact angles, and (d) changes of bubble mass.

of stable equilibrium nanobubbles on these homogeneous substrates. Figure 5(a) shows that the critical heights are less than 100 nm for the hydrophobic substrates besides $\theta_0 = 30^\circ$. Figure 5(b) shows that all the critical contact angles are close to 20°. These results agree with the typical ranges of height and contact angle of nanobubble, and explain, in a certain degree, the weak dependence of the nanobubble contact angle on the substrate wettability observed in experiments [7–14].

Finally, we compare the dynamic evolutions of surface nanobubbles computed by the present study and the pinning model [20,21] as shown in Fig. 6. The nanobubbles have the initial footprint radius $L = 50$, 100, 150, and 200 nm, and the oversaturation takes $\zeta = 1$. In the present study, the surface nanobubbles with different footprint radii evolve to the identical stable nanobubble. On the contrary, with the constant footprint radii, the surface nanobubbles in the pinning model evolve to different equilibrium heights and contact angles [20,21]. The pinning model achieves only the diffusive equilibrium, whereas the present study achieves both the diffusive and mechanical equilibriums. The pinned nanobubbles reach the stable state faster than those in the present study; when the adsorption effect is considered, the inner pressure is lower, and then the gas diffusion across the liquid-bubble interface is slowed down [22].

## IV. CONCLUSIONS

In summary, we propose a model to evaluate the dynamics and stability of surface nanobubbles by integrating the gas diffusion mechanism, the hydrophobic attraction potential, and the gas adsorption effect. It demonstrates the state transition from the stable nanobubbles to unstable microbubbles on

homogeneous substrates. The dynamic evolutions show that the bubble size and environmental oversaturation determine the nanobubble behaviors, namely growth, stability, shrinkage, or dissolution. Except the stable equilibrium nanobubbles, any other surface bubbles are in unstable equilibrium or nonequilibrium state on a homogeneous surface. Their stabilization has three routes: shrinking or growing to the stable equilibrium, otherwise relying on contact line pinning. Thus, contact line pinning can greatly expand the stable range of surface bubbles. The dynamic calculations in this paper only treat gas transport in the vicinity of the nanobubble; when gas transport is considered to equilibrate the bulk liquid with an open environment, the dynamics of surface nanobubbles can achieve to be consistent with experimental response timescale [20,21,24,36].

## ACKNOWLEDGMENTS

This work was supported by the National Natural Science Foundation of China (Grants No. 12272100, No. 11862003, No. 12005284, No. 12022508 and No. 12074394), the Key Research Program of the Chinese Academy of Sciences (No. QYZDJ-SSW-SLH019), and the Innovation Project of Guangxi Graduate Education (No. YCBZ2022065).

[1] D. Lohse and X. Zhang, Surface nanobubbles and nanodroplets, Rev. Mod. Phys. **87**, 981 (2015).
[2] S. Lou, Z. Ouyang, Y. Zhang, X. Li, J. Hu, M. Li, and F. Yang, Nanobubbles on solid surface imaged by atomic force microscopy, J. Vac. Sci. Technol. B **18**, 2573 (2000).
[3] N. Ishida, T. Inoue, M. Miyahara, and K. Higashitani, Nano bubbles on a hydrophobic surface in water observed by tapping-mode atomic force microscopy, Langmuir **16**, 6377 (2000).
[4] M. Alheshibri, J. Qian, M. Jehannin, and V. S. J. Craig, A history of nanobubbles, Langmuir **32**, 11086 (2016).
[5] B. H. Tan, H. An, and C. D. Ohl, Stability of surface and bulk nanobubbles, Curr. Opin. Colloid Interface Sci. **53**, 101428 (2021).
[6] L. Zhou, S. Wang, L. Zhang, and J. Hu, Generation and stability of bulk nanobubbles: A review and perspective, Curr. Opin. Colloid Interface Sci. **53**, 101439 (2021).
[7] L. Zhang, C. Wang, R. Tai, J. Hu, and H. Fang, The morphology and stability of nanoscopic gas states at water/solid interfaces, Chem. Phys. Chem. **13**, 2188 (2012).
[8] X. H. Zhang, N. Maeda, and V. S. J. Craig, Physical properties of nanobubbles on hydrophobic surfaces in water and aqueous solutions, Langmuir **22**, 5025 (2006).
[9] X. H. Zhang, A. Quinn, and W. A. Ducker, Nanobubbles at the interface between water and a hydrophobic solid, Langmuir **24**, 4756 (2008).
[10] L. Zhang, X. Zhang, C. Fan, Y. Zhang, and J. Hu, Nanoscale multiple gaseous layers on a hydrophobic surface, Langmuir **25**, 8860 (2009).
[11] B. M. Borkent, S. de Beer, F. Mugele, and D. Lohse, On the shape of surface nanobubbles, Langmuir **26**, 260 (2010).
[12] B. Song, W. Walczyk, and H. Schönherr, Contact angles of surface nanobubbles on mixed self-assembled monolayers with systematically varied macroscopic wettability by atomic force microscopy, Langmuir **27**, 8223 (2011).
[13] B. H. Tan, H. An, and C. D. Ohl, Resolving the Pinning Force of Nanobubbles with Optical Microscopy, Phys. Rev. Lett. **118**, 054501 (2017).
[14] B. Zhao, X. Wang, S. Wang, R. Tai, L. Zhang, and J. Hu, In situ measurement of contact angles and surface tensions of interfacial nanobubbles in ethanol aqueous solutions, Soft Matter **12**, 3303 (2016).
[15] S. Ljunggren and J. C. Eriksson, The lifetime of a colloid-sized gas bubble in water and the cause of the hydrophobic attraction, Colloids Surf., A **129-130**, 151 (1997).
[16] P. S. Epstein and M. S. Plesset, On the stability of gas bubbles in liquid-gas solutions, J. Chem. Phys. **18**, 1505 (1950).

[17] B. H. Tan, H. An, and C. D. Ohl, How Bulk Nanobubbles Might Survive, Phys. Rev. Lett. **124**, 134503 (2020).
[18] P. B. Duncan and D. Needham, Test of the epstein-plesset model for gas microparticle dissolution in aqueous media: Effect of surface tension and gas undersaturation in solution, Langmuir **20**, 2567 (2004).
[19] Y. Liu and X. Zhang, Nanobubble stability induced by contact line pinning, J. Chem. Phys. **138**, 014706 (2013).
[20] D. Lohse and X. Zhang, Pinning and gas oversaturation imply stable single surface nanobubbles, Phys. Rev. E **91**, 031003(R) (2015).
[21] B. H. Tan, H. An, and C. D. Ohl, Surface Nanobubbles Are Stabilized by Hydrophobic Attraction, Phys. Rev. Lett. **120**, 164502 (2018).
[22] N. D. Petsev, L. G. Leal, and M. S. Shell, Universal Gas Adsorption Mechanism for Flat Nanobubble Morphologies, Phys. Rev. Lett. **125**, 146101 (2020).
[23] Z. Guo, X. Wang, and X. Zhang, Stability of surface nanobubbles without contact line pinning, Langmuir **35**, 8482 (2019).
[24] J. H. Weijs and D. Lohse, Why Surface Nanobubbles Live for Hours, Phys. Rev. Lett. **110**, 054501 (2013).
[25] X. Zhang, D. Y. C. Chan, D. Wang, and N. Maeda, Stability of interfacial nanobubbles, Langmuir **29**, 1017 (2013).
[26] P. Attard, Pinning down the reasons for the size, shape, and stability of nanobubbles, Langmuir **32**, 11138 (2016).
[27] Y. Liu and X. Zhang, A unified mechanism for the stability of surface nanobubbles: Contact line pinning and supersaturation, J. Chem. Phys. **141**, 134702 (2014).
[28] C. U. Chan, M. Arora, and C. D. Ohl, Coalescence, growth, and stability of surface-attached nanobubbles, Langmuir **31**, 7041 (2015).
[29] H. An, B. H. Tan, Q. Zeng, and C. D. Ohl, Stability of nanobubbles formed at the interface between cold water and hot highly oriented pyrolytic graphite, Langmuir **32**, 11212 (2016).
[30] J. Qian, V. S. J. Craig, and M. Jehannin, Long-term stability of surface nanobubbles in undersaturated aqueous solution, Langmuir **35**, 718 (2019).
[31] M. P. Brenner and D. Lohse. Dynamic Equilibrium Mechanism for Surface Nanobubble Stabilization, Phys. Rev. Lett. **101**, 214505 (2008).
[32] S. M. Dammer and D. Lohse, Gas Enrichment at Liquid-Wall Interfaces, Phys. Rev. Lett. **96**, 206101 (2006).
[33] X. H. Zhang, A. Khan, and W. A. Ducker. A Nanoscale Gas State, Phys. Rev. Lett. **98**, 136101 (2007).
[34] T. Koishi, S. Yoo, K. Yasuoka, X. C. Zeng, T. Narumi, R. Susukita, A. Kawai, H. Furusawa, A. Suenaga, N. Okimoto, N. Futatsugi and T. Ebisuzaki, Nanoscale Hydrophobic Interaction and Nanobubble Nucleation, Phys. Rev. Lett. **93**, 185701 (2004).
[35] M. Tortora, S. Meloni, B. H. Tan, A. Giacomello, C. D. Ohl, and C. M. Casciola, The interplay among gas, liquid and solid interactions determines the stability of surface nanobubbles, Nanoscale **12**, 22698 (2020).
[36] B. H. Tan, H. An, and C. D. Ohl, Stability, Dynamics, and Tolerance to Undersaturation of Surface Nanobubbles, Phys. Rev. Lett. **122**, 134502 (2019).
[37] H. An, G. Liu, R. Atkin, and V. S. J. Craig, Surface nanobubbles in nonaqueous media: Looking for nanobubbles in DMSO, formamide, Propylene Carbonate, Ethylammonium Nitrate, and Propylammonium Nitrate, ACS Nano **9**, 7596 (2015).
[38] D. S. Bull, N. Nelson, D. Konetski, C. N. Bowman, D. K. Schwartz, and A. P. Goodwin, Contact line pinning is not required for nanobubble stability on copolymer brushes, J. Phys. Chem. Lett. **9**, 4239 (2018).
[39] Y. X. Chen, Y. L. Chen, and T. H. Yen, Investigating interfacial effects on surface nanobubbles without pinning using molecular dynamics simulation, Langmuir **34**, 15360 (2018).
[40] R. D. Deegan, O. Bakajin, T. F. Dupont, G. Huber, S. R. Nagel, and T. A. Witten, Capillary flow as the cause of ring stains from dried liquid drops, Nature (London) **389**, 827 (1997).
[41] Y. O. Popov, Evaporative deposition patterns: Spatial dimensions of the deposit, Phys. Rev. E **71**, 036313 (2005).

[42] S. H. Donaldson *et al.*, Developing a general interaction potential for hydrophobic and hydrophilic interactions, Langmuir **31**, 2051 (2015).
[43] T. Yamashita, and K. Ando, Aeration of water with oxygen microbubbles and its purging effect, J. Fluid Mech. **825**, 16 (2017).
[44] J. C. Fan, J. De Coninck, H. A. Wu, and F. C. Wang, Microscopic Origin of Capillary Force Balance at Contact Line, Phys. Rev. Lett. **124**, 125502 (2020).
[45] Y. Yamaguchi, H. Kusudo, D. Surblys, T. Omori, and G. Kikugawa, Interpretation of Young's equation for a liquid droplet on a flat and smooth solid surface: Mechanical and thermodynamic routes with a simple Lennard-Jones liquid, J. Chem. Phys. **150**, 044701 (2019).
[46] B. v. Szyszkowski, Experimentelle studien Über kapillare eigenschaften der wässerigen Lösungen von fettsäuren, Z. Phys. Chem. (Muenchen, Ger.) **64U**, 385 (1908).
[47] C. Wang, H. Lu, Z. Wang, P. Xiu, B. Zhou, G. Zuo, R. Wan, J. Hu, and H. Fang, Stable Liquid Water Droplet on a Water Monolayer Formed at Room Temperature on Ionic Model Substrates, Phys. Rev. Lett. **103**, 137801 (2009).
[48] S. Maheshwari, M. van der Hoef, X. Zhang, and D. Lohse, Stability of surface nanobubbles: A molecular dynamics study, Langmuir **32**, 11116 (2016).
[49] L. Zhou *et al.*, Ultrahigh density of gas molecules confined in surface nanobubbles in ambient water, J. Am. Chem. Soc. **142**, 5583 (2020).
[50] G. S. Manning, On the thermodynamic stability of bubbles, immiscible droplets, and cavities, Phys. Chem. Chem. Phys. **22**, 17523 (2020).